Some insights into the screech tone of under-expanded supersonic jets using dynamic mode decomposition

Zang B.[1, †], U S Vevek[2, ‡] and New T. H.[3, §]

1. Faculty of Engineering, University of Bristol. United Kingdom BS8 1TR.
[†]Email: nick.zang@bristol.ac.uk
2. School of Mechanical and Aerospace Engineering, Nanyang Technological University, Singapore 639798. [‡]Email: m150086@e.ntu.edu.sg
3. School of Mechanical and Aerospace Engineering, Nanyang Technological University, Singapore 639798. [§]Corresponding author: dthnew@ntu.edu.sg

Abstract

Jet screech is an intense pure tone which has attracted decades of research interest due to its possible detrimental effect to engineering structures. Its modes and closure mechanisms have been investigated analytically, experimentally and numerically, however, there are still outstanding questions on the generation and propagation of instabilities in the near-field region. Recent studies have identified that the instabilities also travel inside the jet potential during the screech process to form the complete feedback loop. Using dynamic mode decomposition on a 3D pressure near-field from large eddy simulation results, the present study examines the viability of the modal decomposition to provide further insights into the screech modes and its associated characteristics and investigates the effect of temperature mixing in jet screech. The results show that the modal decomposition approach identifies very well the helical structure of the screech mode. Furthermore, a method is proposed to reveal the temporal evolution of the dynamic screech mode. It was found that the bulk behaviour of the pressure field at screech frequency propagates backward towards the nozzle exit.

1. Introduction

When operating at off-design conditions, a supersonic jet exhausting into a quiescent ambience undergoes either an over- or under-expansion process, which is characterised by a train of shock cell structures in the jet potential core (Tam, 1995). The formation of shock cells leads to 'shock associated' noise components in supersonic jet noise, namely the broadband shock associated noise (Harper-Bourne and Fisher 1973; Norum and Seiner 1982; Tam 1990; André

et al. 2013; Pérez Arroyo *et al.* 2019) and the screech tone (Powell 1953; Tam and Hu, 1989; Powell *et al.* 1992; Shen and Tam 2002; Edgington-Mitchell *et al.* 2018; Gojon *et al.* 2018; Mancinelli *et al*. 2019), as a direct result of the jet mixing layers interacting with the shock structures. The jet screech is a very intense tone, first observed and reported by Powell (1953), which is often considered detrimental to engineering components due to its ability to induce sonic fatigue failure and structural damages.

The generation of the screech tone has been extensively studied in the literature. Under specific self-resonance conditions, a screeching jet completes an acoustic feedback loop with, firstly the growth of the instability wave within the mixing layer; secondly interaction between the shock and turbulent structures to generate upstream traveling waves (Tam and Hu, 1989); thirdly, propagation of the upstream traveling waves; and lastly re-excitation of the instability waves upon the jet exit, thus closing the loop for screech tone emission. Using shock-refracted wave model, Kandula (2008) argued that the thin shear layer close to the jet exit were receptive to excitations, hence sustaining the intense screech tone. Furthermore, different screech modes, as the jet Mach number increases and screech tone frequency jumps occur, have been identified as the axisymmetric mode (A1 and A2, also referred to as toroidal mode by Tam), flapping mode and helical mode (Powell 1953; Powell *et al.* 1992; Tam 1995). To understand the closure mechanisms for the feedback loops produced from the different screech modes, Shen and Tam (2002) examined the upstream propagation of disturbance waves and suggested the existence of two possible mechanisms. The first mechanism recognized that the amplification of the Kelvin-Helmholtz instabilities in the mixing layer, which subsequently generates upstream-propagating acoustic perturbations outside of the jet shear layer, was re-excited at the nozzle lip (Tam et al., 1986). While the proposed model agreed well with the experimental and numerical results for the A1 axisymmetric mode and the flapping modes, significant differences were found when predicting the A2 axisymmetric and helical mode (Assunção *et al.*, 2019). The second mechanism, proposed later by Tam and Hu (1989), emphasized on a different instability wave, where it can be found both outside of the jet shear layer and inside of the jet potential core. In more recent experiments conducted by Edgington-Mitchell *et al.* (2018), they identified an upstream-traveling instability mode with a negative phase velocity inside of the jet core flows, using a triple-decomposition method based on proper orthogonal decomposition (POD). Mancinelli *et al.* (2019) and Pérez Arroyo *et al.* (2019) also observed similar upstream-traveling modes in their studies of jet screech tone and broadband shock associated noise.

To extract the most dominant dynamics in the near-field of the jet flows and identify the upstream-moving modes, both Edgington-Mitchell *et al.* (2018) and Mancinelli *et al.* (2019) have applied modal decomposition, *i.e.* POD, to the velocity fields. These modal decomposition methods, such as proper orthogonal decomposition (Berkooz et al., 1993) and dynamic mode decomposition (DMD; Schmid, 2010), are powerful analyses tools for identifying the either energetically or statistically important dynamics of the flow and have been utilized successfully to provide further insights into many flow scenarios (Tu *et al.*, 2014), which help enhance significantly our understanding of a given flow phenomenon. Lárusson *et al.* (2014) subjected their URANS (unsteady Reynolds-Averaged Navier-Stokes) pressure field to DMD and found that the dominant frequency from an optimal ranking of the DMD modes agreed very well with the screech frequency, confirming that generation of screech tone is dynamically dominant in the near-field. Gao *et al.* (2017) applied DMD on their numerical simulation results to examine the interaction noise from twin closely-spaced supersonic jets under perfectly expanded condition. The upstream shift of the DMD modes indicated clearly the effect of jet interactions and an early onset of the shear layer instabilities, which provided an elevated level of jet noise. Burak and Andersson (2018) analysed the velocity field results obtained from their large-eddy simulation using DMD and concluded that DMD was able to isolate the screech tone behaviour from the overall jet dynamics.

Compared to experimental characterisation of supersonic jet noise, which are often challenging and costly to perform, high-fidelity numerical modelling, such as large eddy simulation (LES), can provide rich flow field and noise information on the jets, especially so when the jets are operating at 'measurement-difficult' conditions, e.g. highly heated jet (Brès and Lele, 2019). Hence, there has been a growing number of numerical studies investigating the various aspects of supersonic jet noise and improving understanding of the jet noise phenomenon in the past decade, for instances, Liu *et al.* (2009), Gojon *et al.* (2016), Brès *et al.* (2017), Viswanath *et al.* (2017) and Langenais *et al.* (2019), just to name a few. In a most recent review, Brès and Lele (2019) remarked that the advances in the numerical schemes and methods in discretization, meshing, boundary treatments and turbulence modelling have all contributed to the increased accuracy in numerical modelling. Using numerical modelling, a relatively complete near-field pressure and velocity results can be time-marched and collected with sufficiently small sampling frequencies, and subsequently being subjected to modal decomposition methods to extract and identify the salient features relevant to the different jet noise components.

To extend from the previous literature on the DMD studies of supersonic jet noise and shed further lights on the screech modes of under-expanded jet flows, the present study performs the dynamic mode decomposition on the three-dimensional pressure near-field results obtained from large eddy simulations, with a particular focus on the ability of DMD to identify screech modes and capture the corresponding upstream-traveling mechanisms for both an unheated and a heated supersonic jet. Furthermore, by advancing the DMD modes in time, the characteristics of the screech-dominated pressure near-field are further explored. To the authors' knowledge, there has been very few attempts to show the non-axisymmetric structures of a screeching jet using the dominant dynamic mode derived from three-dimensional pressure fields.

2. Numerical methodology

The simulations in this study were performed using an in-house compressible flow solver developed in the OpenFOAM framework. The inviscid fluxes were calculated using an efficient hybrid flux methodology (U S Vevek *et al.*, 2019) that blends a MUSCL-type HLLC flux scheme and a characteristic HLL flux scheme using a modified shock sensor. The spatial reconstruction was performed using a seventh-order finite volume WENO (weighted essentially non-oscillatory) scheme (Jiang and Shu, 1996) that has been implemented using the dimension-by-dimension approach. The present implementation is capable of handling non-uniform block-structured meshes. An adaptive mapping procedure (U S Vevek *et al.*, 2019) was used to enhance the spectral resolution of the WENO reconstruction. The simulations were performed using the implicit LES (iLES) approach (Garnier *et al.*, 1999; Fureby and Grinstein, 1999) whereby the numerical dissipation of the spatial discretization scheme acts as an implicit SGS (sub-grid scale) model that serves to dissipate the energy contained in the eddies that cannot be resolved on the mesh. The viscous fluxes were calculated using a second-order central difference scheme. The explicit third-order TVD (total-variation-diminishing) Runge-Kutta scheme (Gottlieb and Shu, 1998) was used for time integration.

2.1. Case Setup

A schematic of the computational domain for LES is shown in Fig. 1. Since the domain is axisymmetric, only a half-slice is shown. The domain extends $40D$ downstream and $5D$ upstream of the nozzle outlet. Its radial extent varies from $8D$ at the nozzle outlet plane to $10D$ near the end of the domain. A close-up view of the region close to the nozzle outlet is shown at the bottom of the Fig. 1. The nozzle wall thickness is $t_w = 0.5mm$. A small portion of the

nozzle straightening section measuring $0.5D$ in length is retained in the domain since the nozzle lip provides the required receptivity for the acoustic waves (Bodony and Lele, 2008).

Figure 2 shows the mesh topology used for LES with mesh refinements along the shear layer. The streamwise cell spacings, Δx, at various streamwise locations are given in Fig. 2(a). The streamwise cell spacings smoothly vary across the length of the domain. The streamwise resolution near the nozzle exit and the overall mesh size are comparable to the past studies as summarized in Table 1. The near wall spacing at the nozzle outlet is kept at $\Delta y_w = 0.005mm$. Figures 2(b) and 2(c) show the yz plane cross-sections at $x = 0D$ and $x = 40D$, respectively. The core region was meshed using an OH block topology and care was taken to reduce the skewness of cells by smoothening the grid lines near the corners of the central block.

The initial and boundary conditions for the simulations are listed in Table 2. Wave-transmissive boundary conditions were applied at the far-field boundaries to minimize reflection of acoustic waves. The nozzle wall was modelled as an adiabatic, no-slip wall. The boundary conditions for the inlet were sampled from the results of RANS simulations of the CD (converging-diverging) nozzle that were performed earlier using *rhoCentralFoam*, one of the native solvers in OpenFOAM. More details on the CD nozzle geometry and the RANS simulation setup can be found in Wu and New (2017) and Zang *et al.* (2018), respectively. The RANS results showed that the y_+ values close to the nozzle outlet were smaller than 5 for both cases which indicate that the first cell lies within the viscous sub-layer.

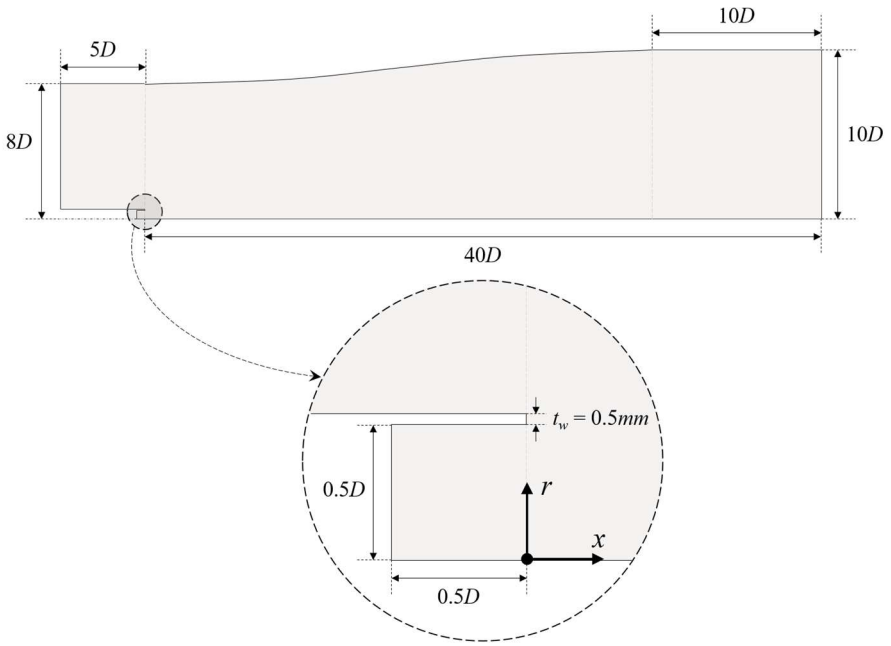

Figure 1. Schematics of the LES computational domain of the under-expanded jets

Study	*Re*	min(Δx)	Total cells ($\times 10^6$)
Daupain *et al.* (2010)	~1*e*6	*D*/40	22
Munday *et al.* (2011)	~5*e*6	*D*/50	–
Mendez *et al.* (2012)	~2*e*5	*D*/80	28
Vuorinen *et al.* (2013)	~2*e*5	*D*/70	12
Li *et al.* (2014)	~1*e*5	*D*/67	27.3
Present	~1*e*6	*D*/64	33.5

Table 1. Comparison of the jet Reynolds number, streamwise cell size (Δx) and total number of cells between past literature and the present study on supersonic jet simulations

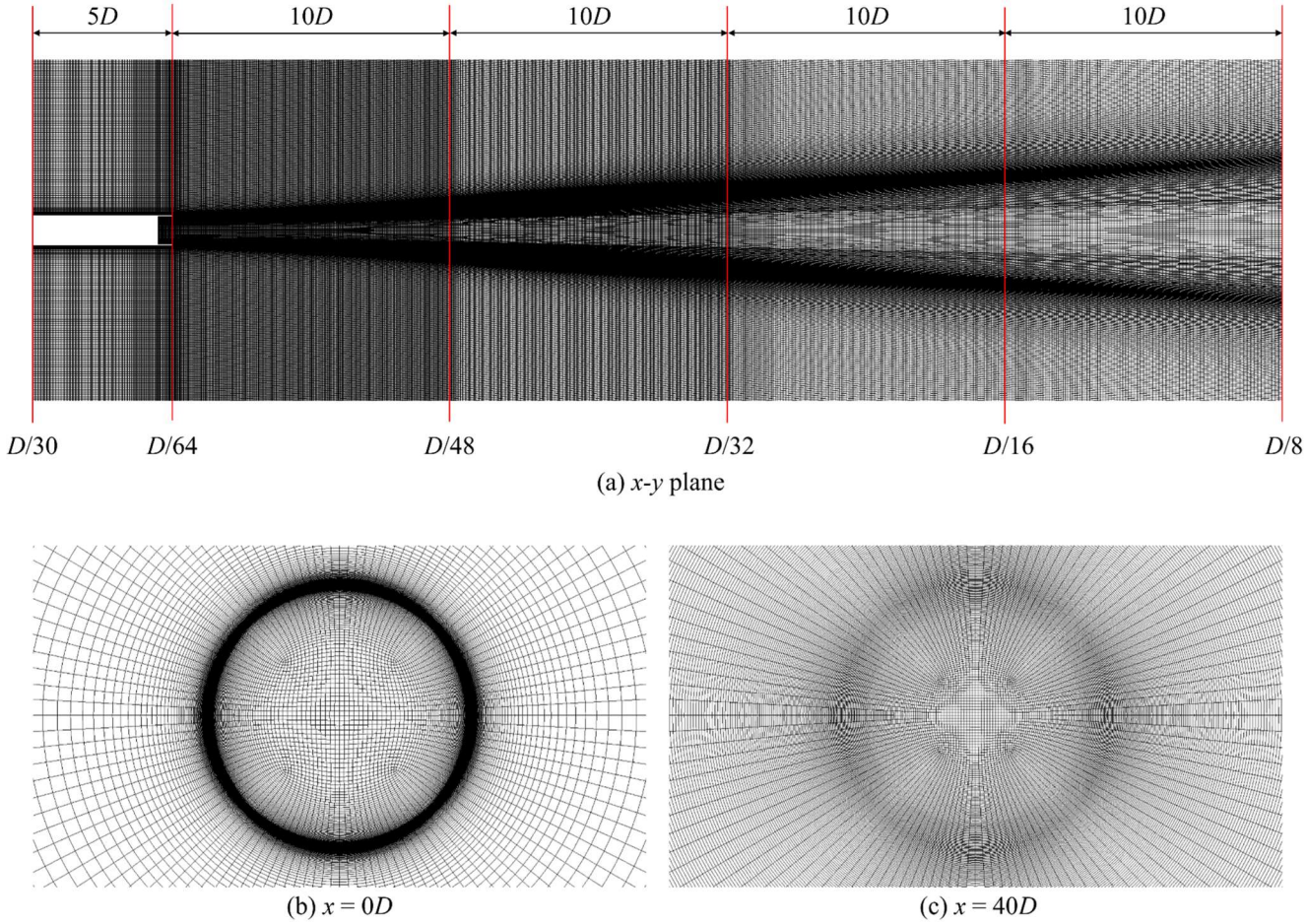

Figure 2. Cross-sectional view of the mesh topology of the LES for (a) entire streamwise domain, (b) yz-plane at the nozzle exit and (c) yz-plane at domain outlet

	pressure, p	velocity, **U**	temperature, T
Initial	100 kPa	(0 0 0) m/s	300 K
Far-field	wave-transmissive	zero-gradient	zero-gradient
Nozzle wall	zero-gradient	no-slip	zero-gradient
Inlet	Sampled from RANS simulations of CD nozzle		

Table 2. Initial and boundary conditions applied to the LES of under-expanded jets

2.2. Jet operating conditions

In earlier studies by Wu and New (2017), Wei *et al.* (2019) and Lim *et al.* (2020), the CD nozzle used in the present simulations was observed to achieve perfect expansion at a nozzle pressure ratio ($\eta = P_t/P_\infty$, where P_t and P_∞ are the total pressure and ambient pressure, respectively) of 3.4 and at $\eta = 5$, the under-expanded jet began to produce intense screech tone. Thus, the nozzle pressure ratio of the under-expanded jet is set at $\eta = P_t/P_\infty = 5$, of which the jet Mach number, M_j, jet velocity, U_j, and fully-expanded to design diameter ratio, D_j/D can then be calculated according to Eq. 1 to 3 shown below:

$$M_j = \sqrt{\frac{2(\eta^{(\gamma-1)/\gamma} - 1)}{\gamma - 1}} \tag{1}$$

$$U_j = M_j \sqrt{\frac{\gamma R T_0}{1 + \frac{1}{2}(\gamma - 1)M_j^2}} \tag{2}$$

$$\frac{D_j}{D} = \left(\frac{1 + \frac{1}{2}(\gamma - 1)M_j^2}{1 + \frac{1}{2}(\gamma - 1)M_d^2}\right)^{\frac{(\gamma+1)}{4(\gamma-1)}} \sqrt{\frac{M_d}{M_j}} \tag{3}$$

where, $\gamma = 1.402$, $M_d = 1.45$, $D = 0.0127m$, $T_\infty = 300K$ and $\eta = 5$. Two temperature ratios of $T_0/T_\infty = 1$ and 2 were chosen for the LES simulations, which corresponds to unheated and heated jets respectively, to firstly examine the validity of the dynamic mode decomposition approach applied to the 3D pressure field under different jet operating conditions, and secondly to investigate the effects of temperature on the temporal evolution of the screech modes. Table 3 lists the various operating conditions of the unheated and heated jets.

The jet characteristic time is defined as $t_j = D/U_j$, where U_j refers to the jet exit velocity. Each LES was performed for a total of $200t_j$. The jet flows were assumed to have settled down to a quasi-steady state by $100t_j$, after which a total of 300 sets of data points were stored for each LES case at intervals of $\Delta t = 10^{-5}s$.

η	T_0/T_∞	T_0	U_j	M_j	D_j
5	1	300 *K*	471 *m/s*	1.708	1.08
5	2	300 *K*	666 *m/s*	1.708	1.08

Table 3. Operating conditions of the unheated and heated under-expanded jets

2.3. Dynamic mode decomposition

The dynamic mode decomposition (DMD) is designed to extract flow structures, which represent (in case of linearized flows) or approximate (in case of non-linear flows) the dominant dynamic behaviour of the measured data. Schmid (2010) first proposed the method based on the snapshots of experimental and numerical data. Different from the companion matrix in the Koopman analysis, Schmid (2010) utilized the numerically more stable approach of single value decomposition to formulate the method, and this has become the defining DMD algorithm. Following the method outlined by Schmid (2010) and Baruk and Andersson (2018), the data sequence, sampled at a frequency of $1/\Delta t$, can be represented in matrix form as:

$$\boldsymbol{Z}_1^N = \{\boldsymbol{z}_0, \boldsymbol{z}_1, \boldsymbol{z}_2 \dots \boldsymbol{z}_{N-1}, \boldsymbol{z}_N\}$$

where each $\boldsymbol{z}_i$ represents a vector of M measurement points, *i.e.* $\boldsymbol{z}_i \in \mathbb{R}^M$. Assuming that the data sequence is generated in a linear time-invariant system, there exists a mapping $\boldsymbol{A}$ that yields:

$$\boldsymbol{z}_t = \boldsymbol{A}\boldsymbol{z}_{t-1}, \qquad \forall\ t = 0, 1, \dots, N-1 \tag{4}$$

The linear operator $\boldsymbol{A}$ describes the dynamics of the system.

Subsequently, two matrices of identical dimensions can be constructed from the snapshots:

$$X \equiv \{\boldsymbol{z}_0 \dots \boldsymbol{z}_{N-1}\} \in \mathbb{R}^{MxN} \text{ and } Y \equiv \{\boldsymbol{z}_1 \dots \boldsymbol{z}_N\} \in \mathbb{R}^{MxN}$$

And the matrix X can be factorised with the single value decomposition as:

$$X = U\Sigma V^* \tag{5}$$

Note that U and V contains the spatial modes (i.e. the proper orthogonal decomposition of the snapshots in matrix X) and the temporal information, respectively. By projecting the linear operator $\boldsymbol{A}$ onto the basis spanned by POD modes of X, the optimal approximation $\widetilde{\boldsymbol{A}}$ to the linear operator $\boldsymbol{A}$ can be determined using Eq. 5:

$$\widetilde{\boldsymbol{A}} = U^{*}\boldsymbol{A}U = U^{*}YV\Sigma^{-1} \tag{6}$$

Finally, the dynamic modes of the snapshots ϕ_i are calculated by solving the eigen-value problem and projecting the eigenvectors back onto the U basis as:

$$\widetilde{\boldsymbol{A}}\boldsymbol{\psi}_i = \lambda_i\boldsymbol{\psi}_i \quad \text{and} \quad \boldsymbol{\phi}_i = U\boldsymbol{\omega}_i \tag{7}$$

For the present LES results, the pressure near-field data were used to construct the $\boldsymbol{Z}$ matrices. It is also worthwhile mentioning that the modes can be further scaled and weighted by solving an optimization problem involving the Vandermonde matrix constructed from $\widetilde{\boldsymbol{A}}$. Nevertheless, the screech tone is an intense and discrete tone, which if present, can be clearly identified from the near-field pressure spectrum. Therefore, no 'ranking' of the DMD modes have been carried out in the following analyses. Instead, the time evolution of a single mode is scrutinized in this work. The pressure field $\boldsymbol{z}_0$ can be approximately reconstructed from the eigenvectors $\boldsymbol{\phi}_i$ as:

$$\boldsymbol{z}_0 \approx \sum_{i=1}^{N} \alpha_i\boldsymbol{\phi}_i \tag{8}$$

where α_i are the amplitudes of the modes at $t = 0$. From Eq. 4, it follows that

$$\boldsymbol{z}(n\Delta t) = \boldsymbol{z}_n \approx \boldsymbol{A}^n\boldsymbol{z}_0 = \sum_{i=1}^{N} \alpha_i\lambda_i^n\boldsymbol{\phi}_i \tag{9}$$

whereby the result on the right is obtained from the definition $\boldsymbol{A}\boldsymbol{\phi}_i = \lambda_i\boldsymbol{\phi}_i$. The above result can be generalized for any arbitrary time t (not only integer multiples of Δt) as given below:

$$\boldsymbol{z}(t) \approx \sum_{i=1}^{N} \alpha_i \exp\left(\ln(\lambda_i)\frac{t}{\Delta \mathrm{t}}\right)\boldsymbol{\phi}_i \tag{10}$$

Focusing on a single mode i, its temporal evolution of the mode, denoted as $\boldsymbol{\phi}_{\tau,i}$, is captured by the following term:

$$\boldsymbol{\phi}_{\tau,i} = \exp\left(\ln(\lambda_i)\frac{t}{\Delta \mathrm{t}}\right)\boldsymbol{\phi}_i \tag{11}$$

Expressing $\lambda_i = e^{j\theta_i}$ (i.e. eigenvalue lies on the unit circle), the period of the mode is given by $T_i = \frac{2\pi\Delta t}{\theta_i}$. Using this result, Eq. 11 simplifies to the following:

$$\boldsymbol{\phi}_{\tau,i} = \exp\left(j\frac{2\pi t}{T_i}\right)\boldsymbol{\phi}_i \tag{12}$$

Eq. 12 can be used to capture the evolution of the mode at several instants over its period $t \in [0, T_i]$ at arbitrarily small intervals.

3. Results and discussion

3.1. Shock cell and time-frequency spectrum validation

Before discussing the LES results and applying modal decomposition to its pressure and velocity fields to further investigate the screech tone behaviour, it is essential to first examine the jet flows captured by the LES and validate not only the overall dynamics, but also its accuracy in time-frequency spectrum with the experiments. Note that limited by the experimental results of the jet flow, only the LES results from unheated jet will be validated with the experimental measurements. Figure 3 shows the comparison between the mean streamwise density gradient, $(\nabla\rho)_z$ from LES ('numerical schlieren') and the schlieren images from experimental work also conducted in-house at similar nozzle pressure ratio of $\eta = 5$. The formation of quasi-periodic shock cells after a series of jet expansion to restore pressure balance is representative of the overall jet dynamics along the potential core. The lengths of the first shock cell, defined as the distance from the nozzle exit to the location where the reflected shock reaches the jet boundary, are shown in Figure 3. It can be seen that there is excellent agreement between LES and experiments for the under-expanded jet.

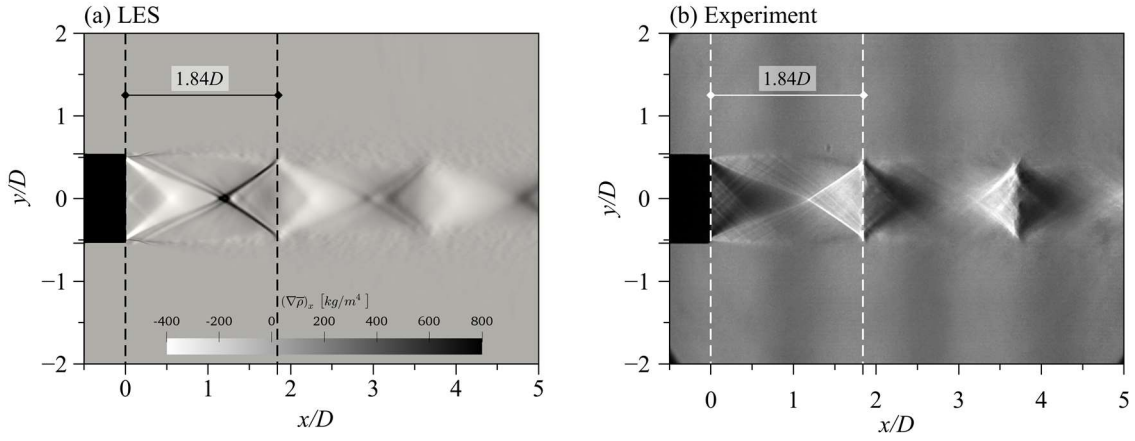

Figure 3. Comparison of shock cell structures and streamwise density gradients from LES with experimental schlieren image

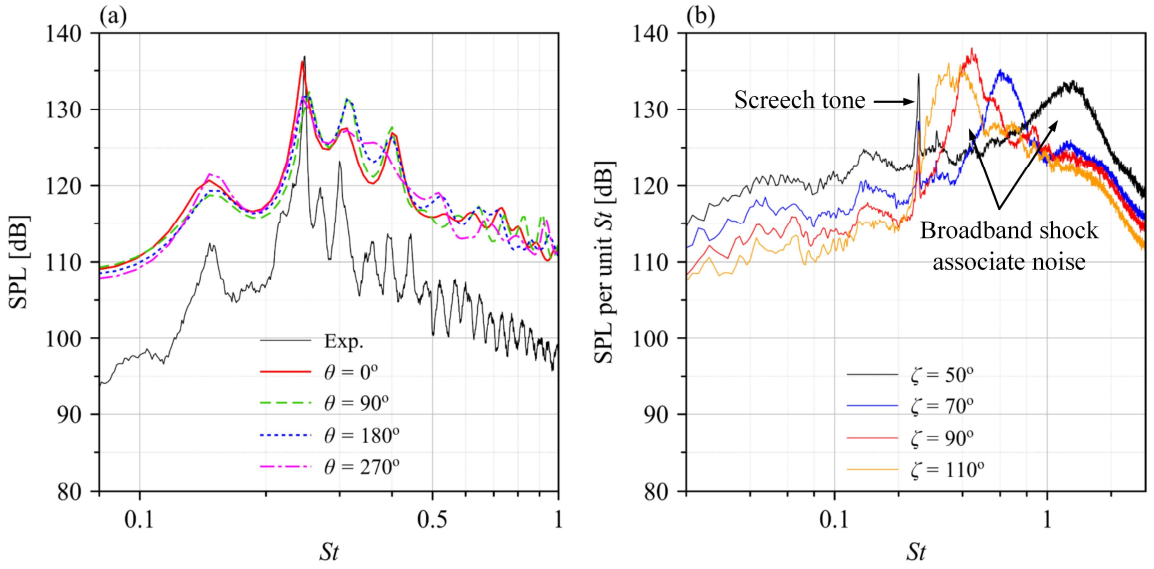

Figure 4. Comparison of the near-field pressure fluctuations at four azimuthal angles with experimental measurement (a) and far-field noise spectra obtained from experimental microphone array (b).

Time-frequency analysis is subsequently performed on the results sampled after the jet have reached quasi steady-state. The probes were placed at four azimuthal locations, $\theta = 0^o, 90^o, 180^o$ and 270^o, at a radial distance of $r = 0.8D$ from the jet centreline line on the nozzle exit plane of $x = 0$. A total of $N = 30001$ time samples were collected. To compensate for the short sample time, the maximum entropy spectral analysis method proposed by Burg (1967) is used to process the sampled unsteady pressure fluctuations. Burg's method is well-suited for processing acoustic data from LES (Larchevêque *et al.* 2004; Levasseur *et al.* 2008) due to its ability to resolve peaks accurately even for short sample times. Figure 4(a) shows the power spectral density of the unsteady pressure fluctuations close to the nozzle, together with experimental results from near-field microphone measurements. The microphone was placed at the same radial distance of $r = 0.8D$ from the jet centreline on the nozzle exit plane at a single azimuthal location. It can be observed from Fig. 4(a) that, despite the short sampling duration compared to experiments, LES captures well the general trend of the time-frequency spectra over the entire Strouhal number range of $0.1 \leq St \leq 1$, where shock-associated jet noise are prominent. Note that the jet Strouhal number is defined as $St = fU_j/D_j$. The three prominent peaks at $St = 0.15, 0.25$ and 0.3 agree very well with the experimental measurements. For the unheated jet at $\eta = 5$, the peak at $St = 0.25$ is identified as the screech tone from the experimental far-field noise measurement as its frequency remains unchanged

with directivity, as shown in Fig. 4(b). All the near- and far-field experimental measurements were conducted by Wei *et al.* (2019) and reproduced for LES validation here.

Examining the comparison between LES and experimental results, while LES captures well the overall trends in the spectra, notable discrepancies exist in terms of spectra magnitude. Results from LES tend to overpredict the power spectra density by about $10dB/St$. The disagreements could possibly stem from the relatively short sample time (Morris *et al.*, 2002). However, the simulation has identified the screech tone relatively accurately, allowing further investigations and analysis into the modes and propagation of screech tone in the under-expanded jets.

3.2. Characterisation of screech tone

Since instabilities associated with the screech modes can be axisymmetric, flapping or helical, it is useful to analyse the cross spectrum of the pressure fluctuations at two different locations close to the jet shear layers, and examine the relative phase between the signals (Gutmark *et al.*, 1989). Given two time series of pressure data $\boldsymbol{p} = \{p_0, p_1, \dots\}$ and $\boldsymbol{q} = \{q_0, q_1, \dots\}$ with a sampling rate of $1/\Delta t$, the normalised cross-correlation coefficient $C \in [-1, 1]$ can be determined as:

$$C(\boldsymbol{p}, \boldsymbol{q}) = \frac{\sum_{k=0}^{N-1} p_k q_{k+M}}{\sqrt{\sum_{k=0}^{N-1} p_k^2} \sqrt{\sum_{k=0}^{N-1} q_k^2}} \tag{13}$$

Here, $N = 10^4$ and the time shift M varies from $0s$ to $0.002s$ at intervals of $10^{-5}s$.

Denoting the pressure time-series at the azimuthal location θ to be $\boldsymbol{p}_\theta$, the cross-correlation coefficients $C(\boldsymbol{p}_0, \boldsymbol{p}_0)$ and $C(\boldsymbol{p}_0, \boldsymbol{p}_{180})$ are computed and plotted in Fig. 5(a). Both cross-spectrum coefficients show periodic behaviour with nearly identical dominant frequency. In addition, temporal evolution of the coefficients appears to be nearly anti-phase. Hence, the dominant frequency and phase difference, $\Delta\varphi$, between the two pairs of coefficients are determined by subjecting the coefficients to fast Fourier-transform (FFT). As can be observed in Fig. 5(b), the dominant frequency, identified by the peak amplitude, occurs at corresponding exactly to the screech frequency. The phase difference between the two coefficients is close to $\Delta\varphi = -180^{\circ}$. The cross-correlation coefficient and its FFT clearly reveals that the screech mode in the unheated jet LES is non-axisymmetric, i.e. flapping or helical.

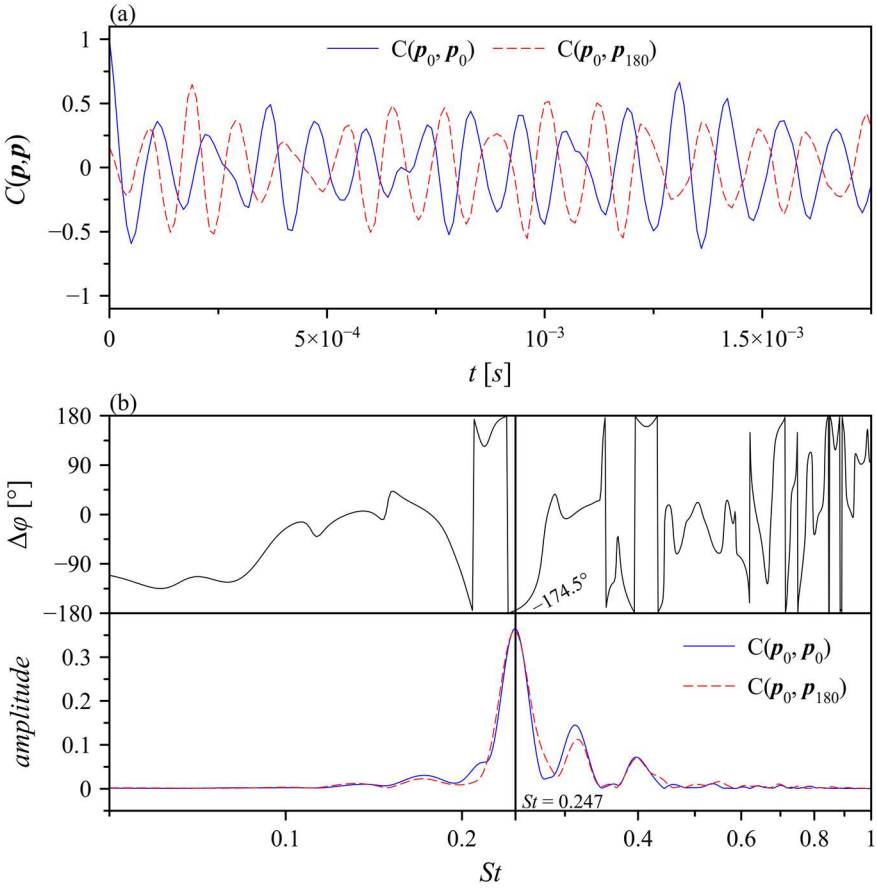

Figure 5. Cross-correlation coefficients $C(\boldsymbol{p},\boldsymbol{p})$ of the time-series pressure data between two probe locations of the unheated jet (a) and FFT spectra and phase differences computed directly from the coefficients C (b).

3.3. Dynamic modes from pressure near-field

As seen from the analysis above, the conventional cross-correlation and time-frequency domain transform may not be able to reveal the full nature of a complex and dynamic process such as the jet screech. Thus, dynamic mode decomposition, which is able to extract the underlying dynamics of the data corresponding to a specific frequency, can offer further insights into these complex flow scenarios. Due to memory restrictions, only a subset of the pressure field encompassing a cylindrical region of radius $3D$ and length $20D$ extending downstream from the nozzle exit plane was used in the DMD analysis with 301 instantaneous pressure field snapshots. To begin with, Fig. 6 shows the distribution of eigenvalues. The eigenvalues are primarily clustered around the circle of unit radius, suggesting a good convergence of the linear dynamic modes to approximate the non-linear process (Burak and Andersson, 2018). Since the jet is considered to be quasi-steady state (*i.e.* the initial transient

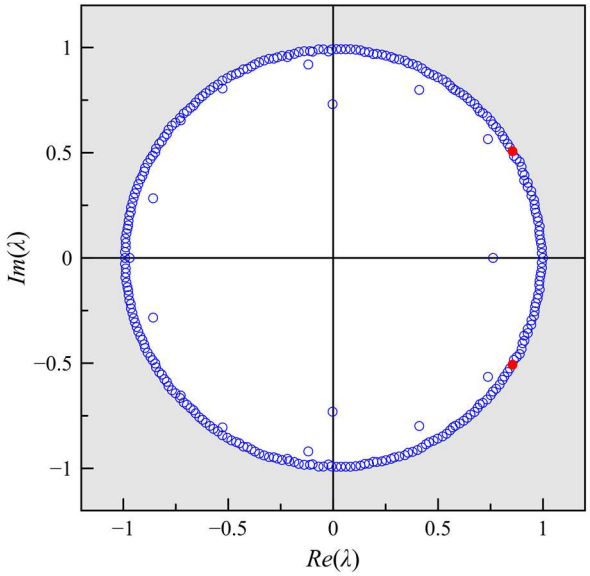

Figure 6. Distribution of Eigenvalues from the DMD modes around a unit circle

effects have already settled and the screech feedback loop has developed and sustained), the majority of the modes are expected to fall onto the unit circle, without significant grow or decay.

The screech mode, which is the dynamic mode having closest frequency to the screech frequency, is then extracted from the DMD analysis, and the isosurfaces S+ and S- are plotted and shown in Fig. 7. The S+ and S- are the positive and negative values of the real part of the mode, i.e. $Re(\boldsymbol{\phi}_i)$. Note that the streamwise cross-section of the DMD mode is superimposed to the isosurfaces to illustrate the acoustic emission of screech tone. There are several notable observations from the dynamically decomposed mode. Firstly, the dominant structure derived from the time-series pressure data is clearly helical, with the positive and negative structures remaining out of phase for all azimuthal angles. Secondly, the helical structure remains relatively stable from $3 \leq x/D \leq 14$. With reference to the shock cell structures (see Fig. 3), the helical structure of the screech mode develops approximately at the end of the second shock cell, where the shock oscillations due to coherent structure roll-ups in the shear layer become pronounced (Suzuki and Lele, 2003). Moreover, the organized helical structure begins to break up at a downstream distance of about $x/D = 14$, which interestingly corresponds quite well with the potential core length of the unheated jet. The relatively stable helical mode over the length of the jet potential core suggests that the screech tone is likely to be produced over a relatively long distance as the shear layer interacts with the shock cells, hence, accurate modelling and prediction of its far-field noise levels would require complete flow field

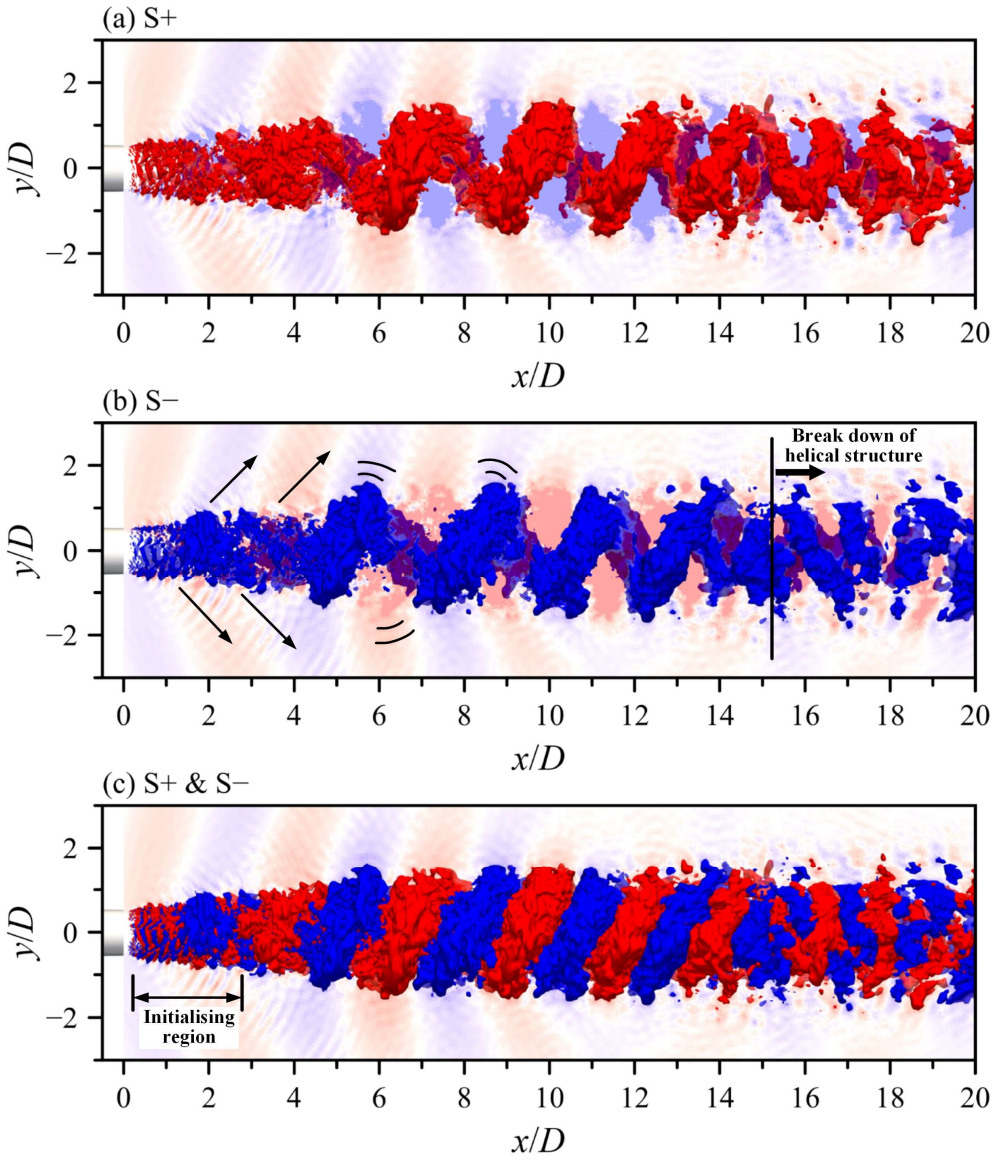

Figure 7. Isosurfaces of the DMD mode at corresponding screech frequency of the unheated jet

information in the near-field. More importantly, the helical structure is not confined merely to the shear layer of the jet but, in fact, initialises both within the jet potential core as well as outside of the jet shear layer, which agrees remarkably well with the recent studies on the propagation of *jet neutral modes*, believed to be responsible for the helical screech mode (Edgington-Mitchell *et al.*, 2018). Thus, the DMD mode reinforces the notion that measurements in the jet potential core is equally important in order to fully understand the screech generation mechanisms.

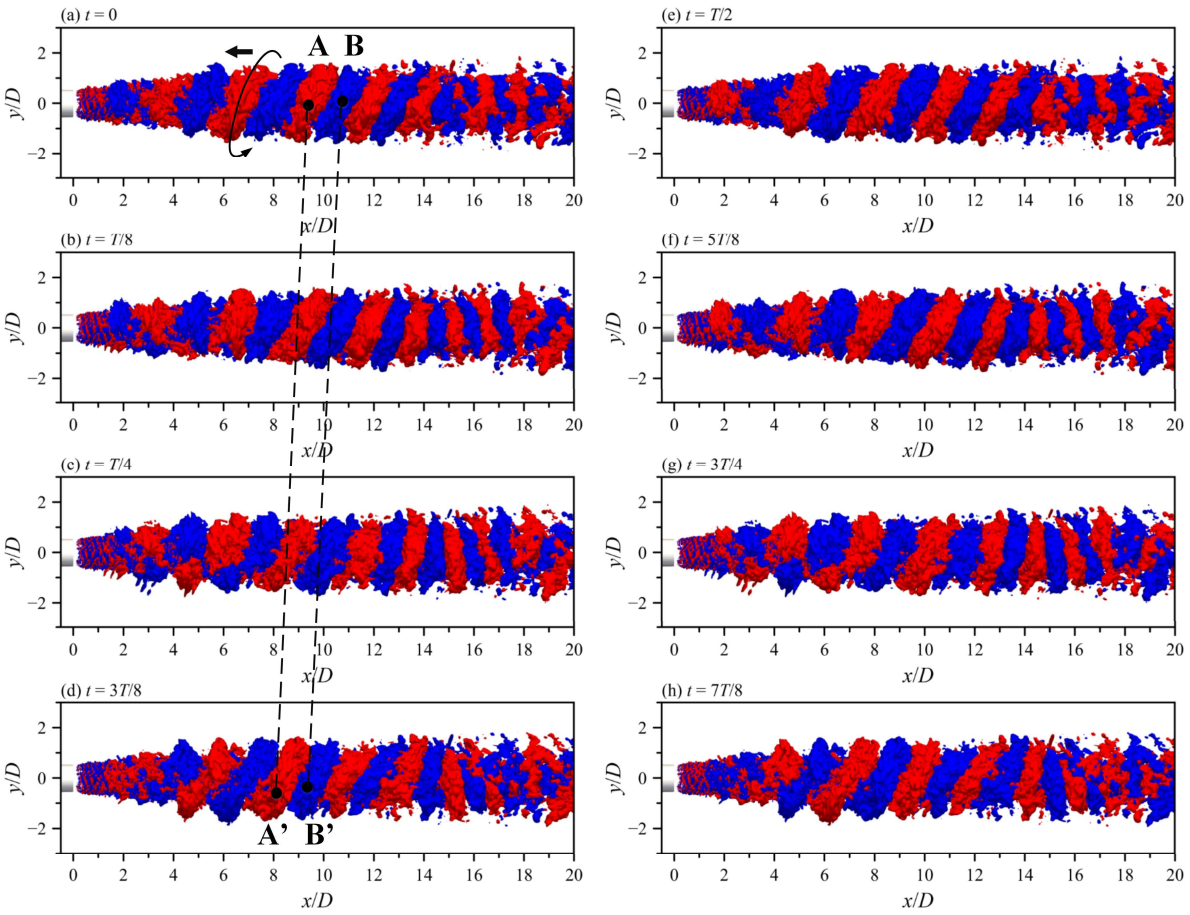

Figure 8. Temporal evolution of the DMD mode corresponding the screech frequency of the unheated jet over a period of T at $T/8$ interval

As proposed in Section 2.3, on top of the spatial DMD mode obtained from the standard analysis, it is possible to obtain the temporal evolution of a given mode by introducing an arbitrary and yet sufficiently small time instant. Following Eq. 12, the temporal evolution of the DMD mode corresponding to the screech frequency over a period T, can be obtained. Figure 8 shows the resulting eight 'instantaneous' modes over the period (i.e. $T/8$ interval). Observing closely the helical structure, it can be observed that both the S+ and S- structures are propagating backward towards the nozzle exit. Note that point A-A' and B-B' indicated in Figs. 8(a) to (d) are pairs of the same feature separated by $T/8$, which have been identified to help track the movement of the helical structure. The dynamics of the temporal evolution of the DMD mode can be more clearly discerned in the movie '*DMD_temporal_unheated*' of the supplementary materials. The backward propagation is both a validation to the DMD analysis applied to the pressure near-field to capture the screech mode, since screech is characterised by the complete feedback loop and a possible means to estimate the bulk propagation speed of the instabilities. For the present analysis, it is estimated that the helical structure propagates at

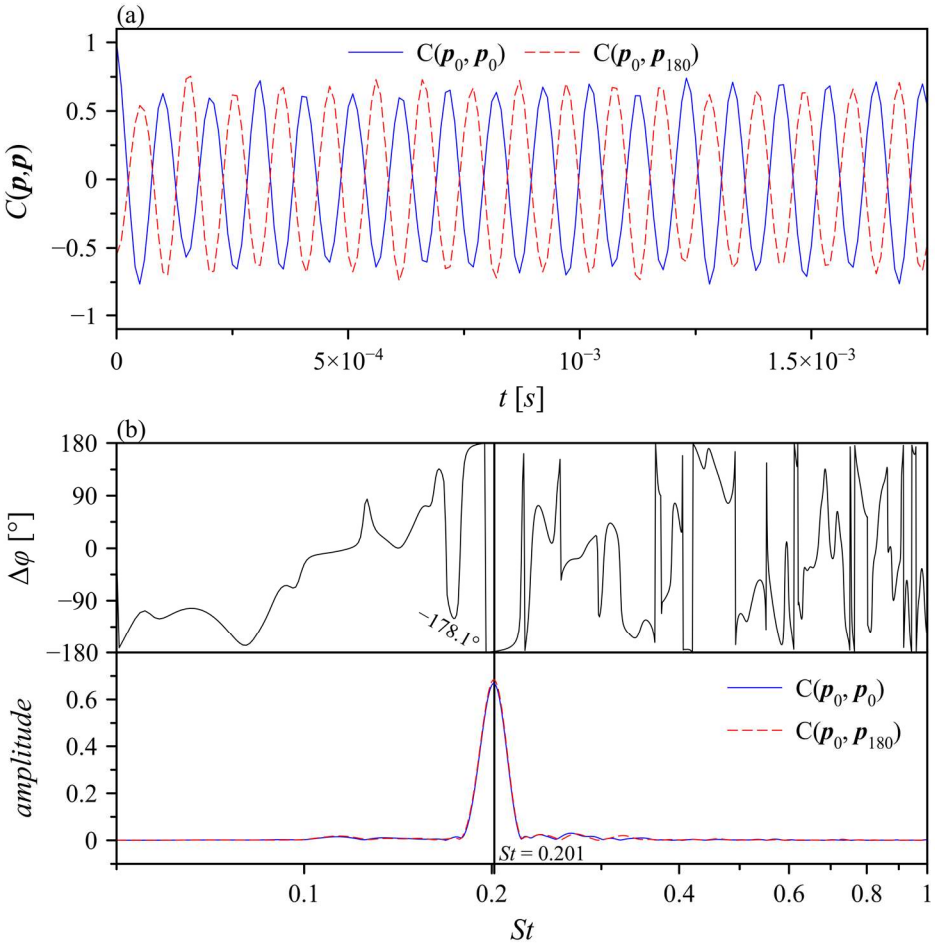

Figure 9. Cross-correlation coefficients $C(\boldsymbol{p},\boldsymbol{p})$ of the time-series pressure data between two probe locations of the heated jet (a) and FFT spectra and phase differences computed directly from the coefficients C (b).

approximately $0.7U_j$, comparable to that of the jet convective velocity (Papamoschou, 1989). However, it should be cautiously noted that additional processing (for instance, image cross-correlation) is necessary to estimate the propagation speed more accurately as the visual-based approach tends to produce noticeable uncertainties.

3.4. Effect of heated jet

Similar to the unheated jet case, LES results of the heated jet with a temperature ratio of $T_0/T_\infty = 2$ were subsequently subjected to the pressure cross-spectrum and DMD analyses, to reaffirm that the present DMD approach is physically meaningful and to examine the effect of temperature mixing to the generation and propagation of jet screech tone. Figure 9 first shows the cross-correlation coefficients between two pairs of probes separated by 180^oazimuthal angle at $x/D = 0$ plane and the corresponding FFT and phase differences determined from

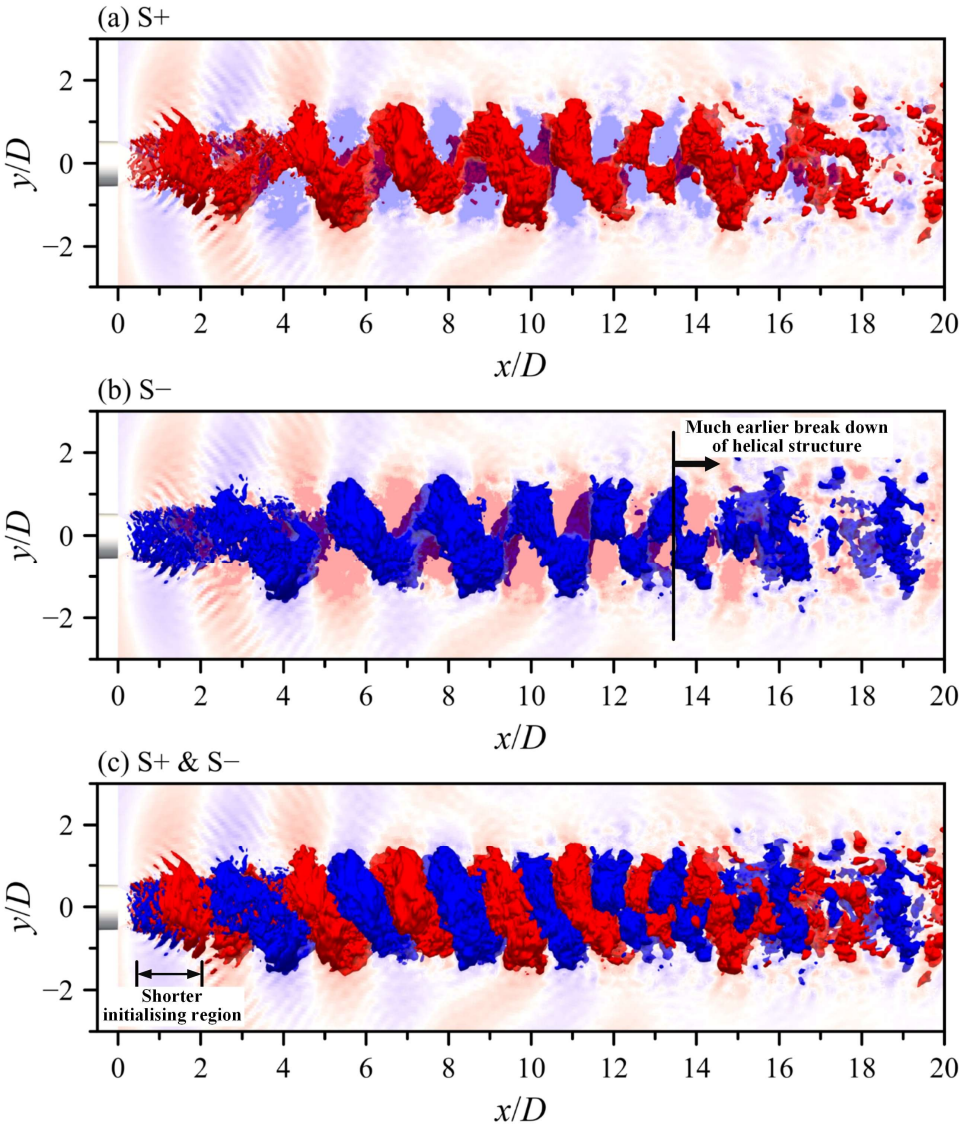

Figure 10. Isosurfaces of the DMD mode at corresponding screech frequency of the unheated jet – this is to be directly compared with Fig. 7

these coefficients. The intense screech tone can be clearly identified to occur at $St = 0.201$, slightly lower than the unheated jet scenario, as expected (Massey *et al.* 1994; Chen *et al.* 2018). The cross-correlation coefficient remains anti-phase, suggesting either a flapping or helical screech mode. Yet, compared to the unheated jet in Fig. 5, the single periodicity associated with jet screech is even more pronounced for the heated jet close to the nozzle exit plane.

Figures 10 and 11 shows the DMD mode associated with the screech mode and its temporal evolution over a period T at $T/8$ intervals, respectively, which can be compared directly with the unheated jet. Although the overall observations from the unheated jet still holds for the heated jet case, it is worthwhile to highlight the differences between the two. Firstly, the helical

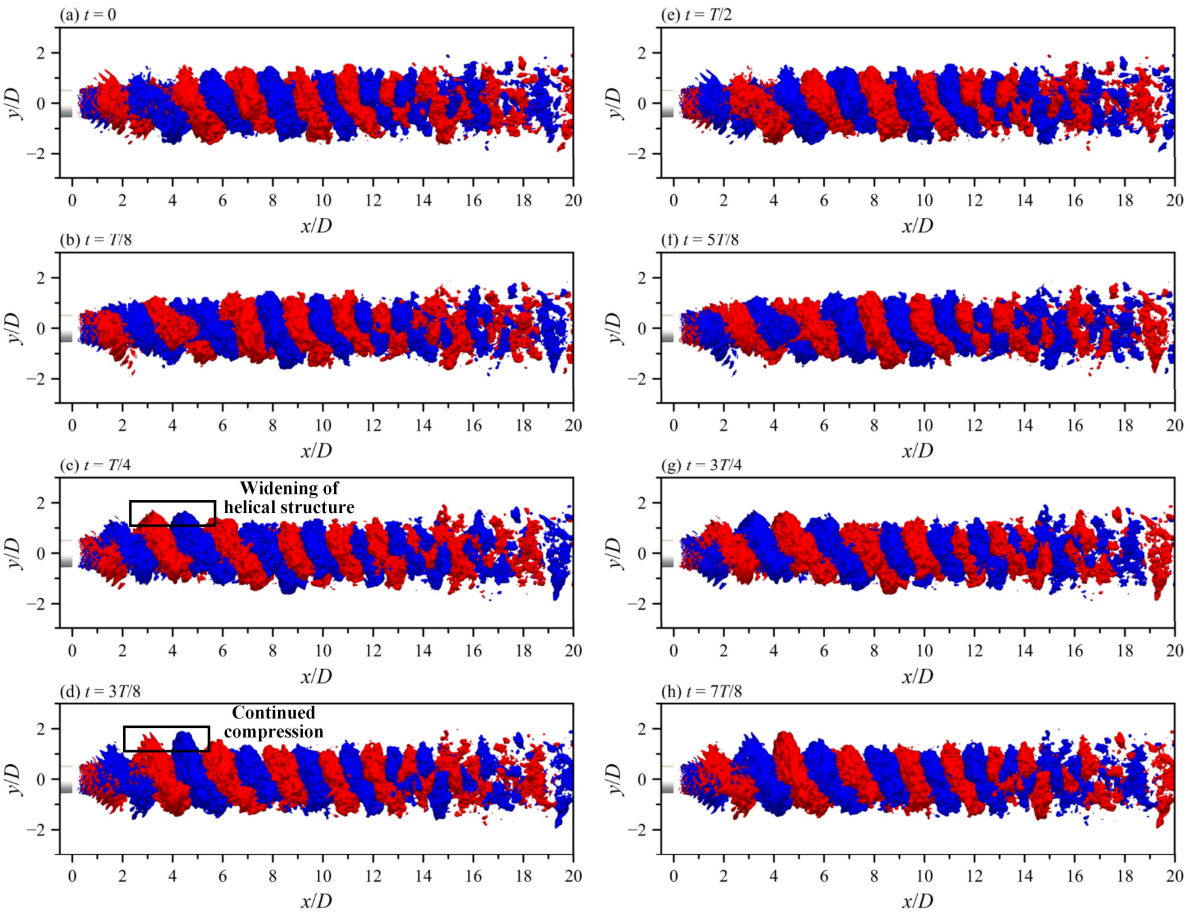

410

411 Figure 11. Temporal evolution of the DMD mode corresponding the screech frequency of the
412 heated jet over a period of T at $T/8$ interval - this is to be compared directly with Fig. 8
413

414 structure develops over a shorter initialising region, suggesting a more intensified growth of
415 the instability waves, which explains that the cross-correlation coefficients show
416 predominantly a single frequency close to the nozzle exit plane. Secondly, the organized helical
417 structure begins to break up at a closer downstream distance than the unheated jet. Hence, it is
418 likely that the temperature mixing has destabilizing effect to the screech mode and the feedback
419 loop. Thirdly, a closer examination of the temporal evolution of the dynamic mode in Fig. 11
420 reveal an intriguing behaviour of the helical structure, where the closer to the nozzle exit, the
421 structures widen and subsequently compress in the spanwise direction with a period of
422 approximately $T/2$. While similar behaviour is absent from the unheated jet, it requires further
423 study to investigate its influence on the generation of screech tone in heated jet.
424

425 ## Conclusion

426 In the present study of unheated and heated supersonic jets, dynamic mode decomposition
427 (DMD) has been applied to the 3D pressure near-field obtained from LES to establish the

validity and effectiveness of DMD analysis in capturing the intense jet acoustics process from pressure field information, and furthermore shed more light on the screech mode and its instability propagation, especially when the temperature mixing is present. The results show that the DMD mode is capable of capturing well the screech modes. In the present jet operating conditions, the helical structure has been clearly identified over the length of the jet potential core. The dynamic mode reveals additional information of the near-field regions where the helical mode is dominant. It is observed that, the instability propagates both within the jet potential core and along the jet shear layer, which agrees very well with recent studies in jet screech phenomenon. Furthermore, a method to obtain the temporal evolution of the DMD mode has been proposed, and it reveals that the bulk behaviour of the jet is dominated by back propagation of the pressure field at screech frequency. Finally, compared to the unheated jet, the growth of the instability wave in heated jet is more intense, as seen from the shorter initialising region of the helical structure. More curiously, there appears to be periodic spanwise widening of the helical structure during the screech process, which requires further investigations in order to better understand the temperature mixing effect.

Data Availability

Some or all data, models, or code that support the findings of this study are available from the corresponding author upon reasonable request.

Acknowledgment

The authors gratefully acknowledge the support provided for the study by the Singapore Ministry of Education AcRF Tier-2 Grant (Grant number: MOE2014-T2-1-002) and School of Mechanical and Aerospace Engineering, Nanyang Technological University, Singapore. The authors would also like to thank Dr Wei X. F. for providing the experimental data.

Reference

1. André, B., Castelain, T. and Baily, C. (2013) “Broadband shock-associated noise in screeching and non-screeching underexpanded supersonic jets”, *AIAA Journal*, 51(3), pp. 665-673.
2. Assunção, T.L., Jaunet, V., Gervais, Y. and Stève, G. (2019) “Closure mechanism investigation of axisymmetric and helical screech modes in underexpanded round jets”, Inter Noise 2019, Madrid.

3. Berkooz, G., Holmes, P. and Lumley, J.L. (1993) “The proper orthogonal decomposition in the analysis of turbulent flows”, *Annual Review of Fluid Mechanics*, 25, pp. 539-575.
4. Bodony, D.J. and Lele. S.K. (2008) “Current status of jet noise predictions using large-eddy simulation”, *AIAA Journal*, 46, pp. 364-380.
5. Brès G.A., Ham F.E., Nichols J.W., Lele S.K. (2017) “Unstructured large eddy simulations of supersonic jets”, *AIAA Journal*. 55, pp. 1164–1184.
6. Brès, G.A. and Lele, S.K. (2019) “Modelling of jet noise: a perspective from large-eddy simulations”, *Philosophical Transactions of the Royal Society A*, 377(2159), 20190081.
7. Burak, M. and Andersson, N. (2018) “Acoustic mode analysis of a supersonic jet”, *AIAA Journal,* 56(1), pp. 279-289.
8. Chen, S., Gojon, R. and Mihaescu, M. (2018) “High-temperature effects on aerodynamic and acoustics characteristics of a rectangular supersonic jet”, AIAA 2018-3303, 2018 AIAA/CEAS Aeroacoustics Conference, Atlanta, GA.
Computational Science, 28, pp. 18-31.
9. Dauptain, A., Cuenot, B. and Gicquel, L.M. (2010) “Large eddy simulation of stable supersonic jet impinging on flat plate”, *AIAA journal*, 48, pp. 2325-2338.
10. Edgington-Mitchell, D., Jaunet, V., Jordan, P., Towne, A., Soria, J., and Honnery, D. R. (2018) “Upstream-travelling acoustic jet modes as a closure mechanism for screech,” *Journal of Fluid Mechanics*, 855, R1.
11. Fureby C. and Grinstein. F.F. (1999) “Monotonically integrated large eddy simulation of free shear flows”, *AIAA Journal*, 37, pp. 544-556.
12. Gao, J, Xu. X. and Li, X. (2018) “Numerical simulation of supersonic twin-jet noise with high-order finite difference scheme”, *AIAA Journal*, 56(1), pp. 290-300.
13. Garnier, E., Mossi, M., Sagaut, P., Comte, P. and Deville, M. (1999) “On the use of shock-capturing schemes for large-eddy simulation”, *Journal of Computational Physics*., 153, pp. 273-311.
14. Gojon, R., Bogey, C. and Marsden, O. (2016) “Investigation of tone generation in ideally expanded supersonic planar impinging jets using large-eddy simulation”, *Journal of Fluid Mechanics*, 808. pp. 90-115.
15. Gojon, R., Bogey, C., and Mihaescu, M. (2018) “Oscillation modes in screeching jets,” *AIAA Journal*, 56(7), pp. 2918-2924.
16. Gottlieb, S. and Shu, C.W. (1998) “Total variation diminishing Runge-Kutta schemes”, *Mathematics of Computation*, 67, pp. 73-85.
17. Gutmark, E., Schadow, K.C. and Bicker, C.J. (1989) “Mode switching in supersonic circular jets”, *Physics of Fluids A: Fluid Dynamics*, 1, pp. 868-873.
18. Harper-Bourne M. and Fisher M.I. (1974) “The noise from shock waves in supersonic jets”, AGARD-CP-131 II: 1-13.

19. J.P. Burg. (1967) “Maximum entropy spectral analysis”, 37th Annual International Meeting, *Society of Exploration Geophysicists*, Oklahoma City.
20. Jiang G.S. and Shu. C.W. (1996) “Efficient implementation of weighted ENO schemes”, *Journal of Computational Physics*, 126, pp. 202-228.
21. Kandula, M. (2008) “Shock-refracted acoustic wave model for screech amplitude in supersonic Jets,” *AIAA Journal*, 46(3), pp. 682-689.
22. Langenais, A., François, V., Troyes, J. and Bailly, C. (2019) “Accurate simulation of the noise generated by a hot supersonic jet including turbulence tripping and nonlinear acoustic propagation”, *Physics of Fluids*, 31:016105.
23. Larchevêque, L., Sagaut, P. Lê, T.-H. and Comte, P. (2004) “Large-eddy simulation of a compressible flow in a three-dimensional open cavity at high Reynolds number”, *Journal of Fluid Mechanics*, 516, pp. 265-301.
24. Lárusson, R., Hafsteinsson, H.E., Andersson, N. and Eriksson, L.-E. (2014) “Investigation of supersonic jet flow using modal decomposition”, AIAA 2014-3312, 20th AIAA/CEAS Aeroacoustics Conference, Atlanta, GA.
25. Levasseur, V., Sagaut, P., Mallet, M. and Chalot. F. (2008) “Unstructured large eddy simulation of the passive control of the flow in a weapon bay”, *Journal of Fluids and Structures*, 24, pp. 1204-1215.
26. Li, X., Yao, W. and Fan, X. (2016) “Large-eddy simulation of time evolution and instability of highly underexpanded sonic jets”, *AIAA Journal*, 54, pp. 3191-3211.
27. Lim, H.D., Wei, X.F., Zang, B., U S Vevek, Mariani, R., New, T.H. and Cui, Y.D. (2020), “Short-time proper orthogonal decomposition of time-resolved schlieren images for transient jet screech characterisation”, *Aerospace Science and Technology*, 107:106276.
28. Liu, J., Kailasanath, K., Ramamurti, R., Munday, D, Gutmark, E and Lohner, R. (2009) “Large-eddy simulations of a supersonic jet and its near-field acoustic properties”, *AIAA Journal,* 47(8), pp.
29. Loh, C.Y. and Hultgren (2002) “Computing jet screech – a complex aeroacoustic feedback system”, NASA Report, TM-2002-211807.
30. Mancinelli, M., jaunet, V., Jordan, P. and Towne, A. (2019) “Screech-tone prediction using upstream-traveling jet modes”, *Experiments in Fluids*, 60:22.
31. Massey, K.C., Ahuja, K.K, Jones III, R.R. and Tam, C.W.K. (1994) “Screech tones of supersonic heated free jets”, AIAA 94-0141, 32nd Aerospace Sciences Meeting and Exhibit, Reno, NV.
32. Mendez, S., Shoeybi, M., Sharma, A., Ham, F.E., Lele, S.K. and Moin, P. (2012) “Large-eddy simulations of perfectly expanded supersonic jets using an unstructured solver”, *AIAA Journal*, 50, pp. 1103-1118.
33. Morris, P.J., Long, L.N., Scheidegger, T.E. and Boluriaan, S. (2002) “Simulations of supersonic jet noise”, *International Journal of Aeroacoustics*. 1, pp. 17-41.

536 34. Munday, D., Gutmark, E., Liu, J. and Kailasanath, K. (2011) "Flow structure and acoustics
537 of supersonic jets from conical convergent-divergent nozzles", *Physics of Fluids*,
538 23:116102.
539 35. Norum, T.D. and Seiner, J.M. (1982) "Measurement of static pressure and far-field
540 acoustics of shock-containing supersonic jets", NASA Report, TM- 84521.
541 36. Pérez Arroyo, C., Daviller, G., Puigt, G., Airiau, C. and Moreau, S. (2019) "Identification
542 of temporal and spatial signatures of broadband shock associated noise", *Shock Waves*, 29
543 (1), pp. 117-134.
544 37. Powell, A. (1953) "On the mechanism of choked jet noise", *Proceedings of the Physical*
545 *Society, Section B*, 66(12), pp. 1039–1056.
546 38. Powell, A., Umeda, Y., and Ishii, R. (1992) "Observations of the oscillation modes of
547 choked circular jets", *The Journal of the Acoustical Society of America*, 92(5), pp. 2823–
548 2836.
549 39. Schmid, P.J. (2010) "Dynamic mode decomposition of numerical and experimental data",
550 *Journal of Fluid Mechanics*, 656, pp. 5-28.
551 40. Shen, H. and Tam, C.K.W. (2002) "Three-dimensional numerical simulation of the jet screech
552 phenomenon", *AIAA Journal*, 40, pp. 33–41.
553 41. Suzuki, T. and Lele, S.K. (2003) "Shock leakage through an unsteady vortex laden mixing
554 layer: application to jet screech", *Journal of Fluid Mechancs*, 490, pp. 139–167.
555 42. Tam, C.K.W. (1990) "Broadband shock associated noise of moderately imperfectly
556 expanded supersonic jets", *Journal of Sound and Vibration*. 140, pp. 55-71.
557 43. Tam, C.K.W. (1995) "Supersonic Jet Noise", *Annual Review of Fluid Mechanics*, 27, pp. 17-
558 43.
559 44. Tam, C.K.W. and Hu, F., (1989) "On the three families of instability waves of high-speed jets",
560 Journal of Fluid Mechanics, 201, pp 447–483.
561 45. Tam, C.K.W., Seiner, J.M., and Yu, J.C. (1986) "Proposed relationship between broadband
562 shock associated noise and screech tones," *Journal of Sound and Vibration*, 110(2), 1986,
563 pp. 309–321.
564 46. Tu, J.H., Rowley, C.W., Luchtenburg, D. M., Brunton, S. L., and Kutz, J. N., "On dynamic
565 mode decomposition: theory and applications", *Journal of Computational Dynamics*, 1(2),
566 pp. 391–421.
567 47. U S Vevek, Zang, B. and New T.H. (2019) "Adaptive mapping for high order WENO
568 methods", *Journal of Computational Physics*, 381, pp. 162-188.
569 48. U S Vevek, Zang, B. and New. T. H. (2019) "An efficient hybrid method for solving Euler
570 equations", *Journal of Scientific Computing*, 81, pp. 732-762.
571 49. Viswanath, K., Johnson, R., Corrigan, A., Kailasanath, K., Mora, P., Baier, F., and Gutmark,
572 E. (2017) "Flow statistics and noise of ideally expanded supersonic rectangular and circular
573 Jets," *AIAA Journal*, 55(10), pp. 1–15.

50. Vuorinen, V. Yu, J., Tirunagari, S., Kaario, O., Larmi, M., Duwig, C. and Boersma, B. (2013) "Large-eddy simulation of highly underexpanded transient gas jets", *Physics of Fluids*, 25:016101.
51. Wei, X.F., Mariani, R. Chua, L.P., Lim, H.D., Lu, Z.B., Cui, Y.D. and New, T.H. (2019) "Mitigation of under-expanded supersonic jet noise through stepped nozzles", *Journal of Sound and Vibration*, 459:114875.
52. Wu, J. and New, T.H. (2017) "An investigation on supersonic bevelled nozzle jets", *Aerospace Science and Technology*. 63, pp. 278–293.
53. Zang, B., U S Vevek, Lim, H.D., Wei, X.F. and New, T.H. (2018) "An assessment of OpenFOAM solver on RANS simulations of round supersonic free jets", *Journal Computational Science,* 28, pp. 18-31.